Available online at www.sciencedirect.com
SCIENCE DIRECT®
Polymer 45 (2004) 2403–2411
polymer
www.elsevier.com/locate/polymer

Embedding poly(styrene sulfonic acid) into PVDF matrix—a new type of proton electrolyte membrane

Ningping Chen, Liang Hong*

Department of Chemical and Environmental Engineering, National University of Singapore, 10 Kent Ridge Crescent, Singapore 119260, Singapore

Received 6 February 2003; received in revised form 27 January 2004; accepted 27 January 2004

Abstract

Hydrophilic polymer segments, consisting of styrene sulfonic acid (SSA) units, were uniformly embedded into hydrophobic poly(vinylidene fluoride) (PVDF) matrix through the mediation of poly(methyl methacrylate) (PMMA) segments, with which SSA segments form a copolymer. Discrete domains (~100 nm) assembled by the SSA segments have been identified throughout the matrix of the membrane, which was prepared through blending of the copolymer P(MMA–SSA) and the PVDF. The thermal stability of the SSA was largely boosted in such hydrophobic environment. This unique matrix structure offers proton conductivity of as high as 10^{-3} S/cm at a low SSA equivalent (0.6 mmol $-SO_3H$/g of membrane), which is accompanied with a low level of water uptake (26%) at ambient temperature. Using this type of polymer membrane as electrolyte, the electrochemical cell possesses obvious capacitive resistance when the membrane is in the anhydride form according to the impedance analysis. However, the capacitive character vanishes when the membrane is hydrated; this response is attributed to the existence of highly dispersed SSA domains in the membrane. This work also analyzes the impedance spectra of the membranes at different hydrated states or with different SSA contents by using an equivalent electrical circuit.

Keywords: Proton electrolyte membrane; Poly(styrene sulfonic acid); Amphiphilic polymer blend

1. Introduction

Nafion® is a type of important perfluorinated polymers used as the proton-exchange membrane (PEM) for a variety of applications, especially as the electrolyte in the hydrogen fuel cell. Possessing a sulfonic acid group at the end of each graft perfluorinated branch, Nafion polymers is able to form a matrix composed of hydrophilic/hydrophobic microdomains spontaneously when a solid matrix is formed via the solution casting technique [1]. It is noteworthy that such a composite structure allows both hydrophilic and hydrophobic domains to fulfill their respective functionalities as a PEM in the hydrogen fuel cell device.

Motivated by the desire to develop cost-effective substitutes for Nafion that is known to take up 20–30% of the total cost of a fuel cell, the usual tactic relies on graft polymerization of styrenic monomers onto a fluorinated polymer matrix and followed by sulfonation [2,3]. It has been found that the lightly or intermediately grafted matrixes contain an uneven distribution of the styrenic groups [4]. This distribution will exert an adverse influence on the sulfonation efficiency and the proton conductivity afterward. Alternatively, a large extent of the grafting and the sulfonation accompanied would cost the resulting membrane its mechanical stability, especially in the hydrated state. Therefore, it is rather difficult to construct a Nafion-like microstructure by means of the graft polymerization.

Assuming a copolymer is designed to consist of two kinds of alternating segments, one of which is miscible with a fluorine-containing polymer, e.g. poly(vinylidene fluoride) (PVDF), and another segment comprises styrene sulfonic acid (SSA) units, a maximum dispersion of the SSA segment in the fluorine polymer matrix could then be achieved depending upon the content of the miscible segment. In this study, poly(methyl methacrylate) (PMMA) was adopted as the segment that is miscible with PVDF, both are in effect miscible in a quite broad range of compositions [5–8]. On the other hand, the MMA can copolymerize with the SSA at any arbitrary monomer ratio. Hence, the MMA segment is an ideal intercession for

* Corresponding author. Tel.: +65-6874-5029; fax: +65-6779-1936.
E-mail address: chehongl@nus.edu.sg (L. Hong).

0032-3861/$ - see front matter © 2004 Elsevier Ltd. All rights reserved.
doi:10.1016/j.polymer.2004.01.047

bringing the SSA into the PVDF. A series of copolymers P(MMA–SSA) with different monomer unit ratios has been synthesized via free radical solution polymerization. The membrane was fabricated by blending the resultant P(MMA–SSA) with the PVDF in an organic solvent and followed by casting. A uniform distribution of nano-scale domains of SSA segments was found throughout the membrane matrix. Hence, this study focused on the understanding of how this unique matrix structure shapes the proton conducting behavior.

2. Experimental

2.1. Chemicals

Methyl methacrylate (Aldrich) was passed through an inhibitor-remover before used. Sodium styrene sulfonate (NaSS, Aldrich) was converted into its acidic form (SSA, *p*-$C_2H_3C_6H_4SO_3H{\cdot}H_2O$) using the ion exchange resin (Amberjet 1200 H $\sim$ 2 equiv. L^{-1}, Aldrich). A DMF solution of NaSS (5 g L^{-1}) was allowed to pass through the packed column of Amberjet 1200 H beads with maintaining the equivalent of proton about 1.5 times as much as Na^+ ions of NaSS. The ion-exchange percentage was 95–97% according to base titration of the solute separated from the eluant via vacuum evaporation to remove DMF. 2,2′-Azobisisobutyronitrile (AIBN, Aldrich) was re-crystallized in methanol before used. *N*,*N*-dimethylforamide (DMF), poly(vinylidene floride) (PVDF) (Aldrich, $M_w = 534,000$) and Nafion®-117 (Aldrich, membrane, 0.007 in.) were used as received.

2.2. Synthesis of composite membranes

2.2.1. Synthesis of the MMA–SSA copolymer

The monomers (MMA and SSA) were dissolved in DMF to obtain a solution with 25 wt% of concentration. A variety of weight ratios of SSA to MMA in the monomer mixture were used to prepare the copolymer. The monomer feed together with the initiator AIBN were charged into a three-neck-round-bottom flask in an oil bath. The polymerization was carried out at 80 °C under magnetic stirring and nitrogen atmosphere for 24 h. The reaction mixture was then poured into a large excess of methanol to precipitate the polymer. The product was filtrated and washed with de-ionized water to remove, if any, the poly(SSA) homo-polymer. After dried in a vacuum oven, the content of SSA in the copolymer was determined using UV spectroscopy at $\lambda = 261$ nm, which was found to be the maximum absorption wavelength of SSA unit in PSSA. A reference curve of absorbance against concentration was plot by using five reference samples of homo-PSSA in DMF, which revealed a very good linearity. The SSA content in the copolymer was determined by the intensity of absorbance at 261 nm, of which the corresponding concentration could be located from the reference curve. The result is listed in Table 1, where the symbol MMA–SSAi : j is used to denote the copolymer, i : j being the weight ratio of MMA to SSA in the monomer feed.

2.2.2. Preparation of the polymer blends

In a typical procedure, a DMF solution containing a MMA–SSA sample and the PVDF with a total concentration of $\sim$20 wt% was prepared. The blending of the two polymers was carried out with assistance of ultrasonic agitation for 2 h. After that, the polymer solution was spread over a glass plate and followed by drying under vacuum at 80 °C for a few days; a composite membrane was then obtained which has a thickness in the range of 02–0.3 mm. Different compositions of the membranes (blends) prepared are listed in Table 2. An abbreviation (DF/MMA–SSAi : j) is used to denote the blends, wherein the weight ratio of PVDF (DF) to the copolymer is equal to unity in all the samples prepared.

2.3. Measurement of the electric conductivity

A special Teflon device was designed in which a round membrane could be sandwiched by the two round stainless steel plates ($\sim$1.5 cm^2) via screwing on the device. Electrical resistance signals were thus taken from the two silver wires connected to the stainless steel electrodes, respectively. The device was placed in a cylindrical chamber where the humidity was maintained by allowing a damp air-flow to pass through the chamber.

2.4. Instrumental

The electrical property of the membranes was determined by AC measurement using an Impedance/-Gain-Phase Analyzer (Solartron SI 1260). Content of SSA in the copolymer was determined by UV/VIS/NIR Spectrometer (Perkin–Elmer Lambda 900). Infrared spectra of the samples were obtained on a BIO-RAD FTS-135 FT-IR spectrometer. The thermal properties of the synthesized membranes were analyzed on a NETZSCH DSC-200 instrument, and the thermogravimetric analysis (TGA) (Instrumental TGA2050) was performed using a scanning rate of 10 deg/min. Morphologies of the membranes were investigated on a scanning electron microscope (JEOL JSM-5600).

3. Results and discussion

3.1. Copolymerization of MMA and SSA

According to the Q–e scheme [9–10], the monomer reactivity ratios (r_1 and r_2) for the copolymerization of styrene and MMA agree very well with the experimental data; an alternating copolymer is resulted. For the

Table 1
Content of SSA (wt%) in copolymer

	MMA–SSA9:1	MMA–SSA8:2	MMA–SSA7:3	MMA–SSA6:4
Calculated according to monomer feed	10	20	30	40
UV measurement	11.4	18.6	27.5	36.4

copolymerization of SSA and MMA, lacking in $Q-e$ values for SSA makes it not possible to calculate the monomer reactivity ratios. However, as far as the resonance and polar effects are concerned, the nitro group functions very similarly to the sulfonic group. Hence, it should be acceptable that the $Q-e$ values of 4-nitro-styrene and MMA are analogous to that of MMA and SSA (Table 3). With this approximation, MMA reactivity ratio r_1 equals about 0.48, while the SSA reactivity ratio r_2 is about 1.27, and then the product $r_1 r_2$ equals 0.61. This means that the resulting copolymer will be in between ideal and alternative copolymer and SSA prefers to form longer segment in the copolymer than MMA does. Statistically, the length of SSA segments in the copolymer depends on the content of SSA in the monomer feed. A previous study [11] on the copolymerization of SSA and styrene showed that a block copolymer was resulted and the distribution of SSA blocks in the copolymer was affected by the monomer ratio. As styrene and MMA have very similar reactivity in the free-radical copolymerization, a combination of either one of them with SSA would yield analogous copolymer structures.

Fig. 1 shows the IR spectrum of MMA–SSA9:1 with reference to the IR spectrum of PMMA. The former did not display the characteristic (asymmetric and symmetric) vibration absorption bands of $-SO_3H$ group in the range of 1100–1350 cm^{-1} because of a low SSA content (~11%) in the copolymer. Since the C–O vibration of the MMA units occurs also in this range, the band observed here was actually an overlap of S=O and C–O absorptions, which thus presented a different shape from the adsorption bands of the pristine PMMA in the same vibration range. Moreover, UV analysis (Table 1) showed that the SSA content in the copolymer was somewhat lower in comparison with that in the monomer feed in most cases; this is because the copolymerization might also produce a small fraction of the copolymer chains containing prevalent SSA contents, which were removed during the purification process.

3.2. Thermal stability of the DF/MMA–SSA membrane

The profiles of thermogravimetric analysis of MMA–SSA7:3 and DF/MMA–SSA7:3 are shown in Fig. 2 as an example. The experiment was conducted in nitrogen atmosphere, and both samples had been dried under vacuum at 80 °C for 2 days before testing. The TGA profile of MMA–SSA7:3 consists of several weight loss stages; it is quite different from that of the pristine PMMA which exhibits only a single sharp decomposition curve. For copolymer MMA–SSA7:3, the first weight loss stage occurred within the range 170–220 °C, accounting for about 14% of weight loss. This value is roughly equal to the mass content of sulfonic groups in the copolymer. Therefore, this degradation stage can be attributed to the elimination of sulfonic groups. Similar phenomenon has been observed in other polymer systems [12,13]. When poly(styrene sulfonic acid) is grafted to PVDF, the onset point of degradation is at about 220 °C [12], while for the sulfonated polybenzimidazole (PBI), this value is around 350 °C [13]. In light of the difference between the structures of benzimidazole and styrene, the desulfonation temperature is affected by the rigidity of the molecular structure to which sulfonic acid is anchored. Benzimidazole unit should be much less susceptible than styrenic unit to the thermal-caused vibration. Similarly, the boost of the desulfonation temperature (from 220 to 380 °C in Fig. 2) could be solely attributed to the mixing of MMA–SSA7:3 with the PVDF, which leads to the formation of an ordered SSA assembly as proposed in Fig. 3. The ordered packing of SSA units could enhance the thermal stability of the sulfonic acid group due to geometric fixation and the formation of a large extent of hydrogen bonding.

A further evidence for the existence of such an ordered assembly could be found from the shift of infrared vibration frequency of S=O bonds of the sulfonic acid group. It has been known that asymmetric and symmetric S=O stretching vibration bands (around 1355 and 1155 cm^{-1}) normally appear on the IR spectra of aromatic rings bearing sulfonic acid group(s). From the IR spectra of small-molecular-weight aromatic sulfonic acid compounds [14], a general

Table 2
Composition of the blended membranes of DF/MMA–SSA

	DF/MMAS–SSA9:1	DF/MMA–SSA8:2	DF/MMA–SSA7:3	DF/MMA–SSA6:4	Nafion®-117
SSA (wt%)	6.1	10.3	16.0	22.3	
$H^{\oplus}$ (mmol g^{-1})	0.3	0.6	0.9	1.2	0.9

Table 3
The monomer reaction ratios

	Q	*e*	MMA/St		MMA/SSA	
			r1	r2	r1	r2
Methyl methacrylate	0.78	0.40	0.48		0.49 ≥	
Styrene	1.00	−0.80		0.49		
p-Nitrostyrene	1.63	0.39				
p-Styrene sulfonic acid	≥1.63	≈0.39				≥1.27

trend could be identified: the crystallization always causes a decrease in the frequencies of the S=O IR absorption bands. This could be linked to an extensive of hydrogen bonding among sulfonic acid groups, which becomes possible only in a crystalline lattice. Applying this view, the fact that S=O frequencies of the SSA unit in the polymer blend DF/MMA–SSA6:4 reduced to 1188 and 1123 cm^{-1} (Fig. 4) is an evidence for the possible ordered assembling shown in Fig. 3, although detailed spatial arrangement of SSA units is still unclear. Moreover, on the spectrum of DF/MMA–SSA6:4, the two absorption bands of sulfonic acid group can be clearly identified while they cannot be seen in the spectrum of DF/MMA–SSA9:1 due to very low content of SSA (~6%). The peak (1136 cm^{-1}) appearing in this range is regarded as an addition of C–O and C–F vibration absorptions. Furthermore, as the MMA and the SSA interact very differently with the DF: a hydrophobic repulsion between the DF and the SSA is expected as depicted in Fig. 5, which might serve as a driving force to the assembling of SSA segments.

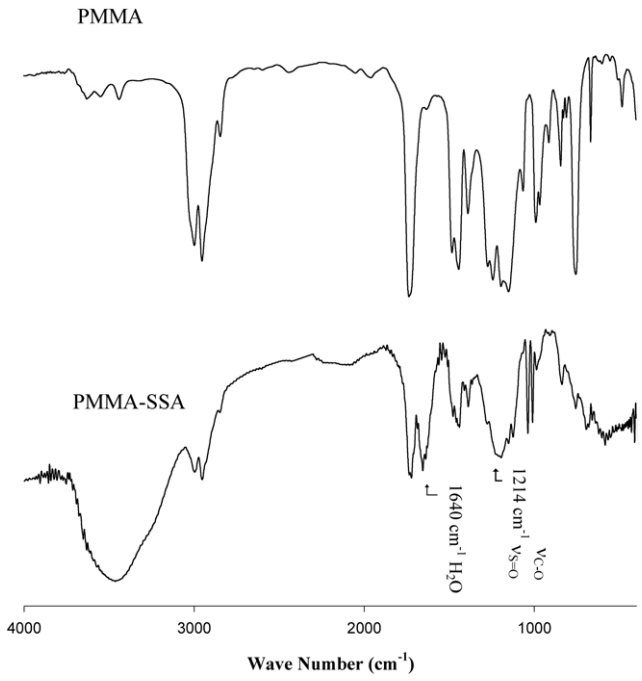

Fig. 1. FT-ir spectra of PMMA and MMA–SSA9:1.

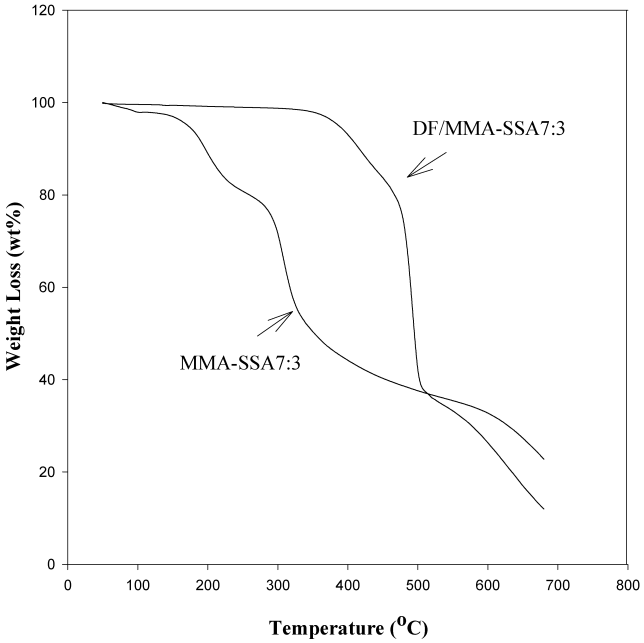

Fig. 2. TGA analysis of blend DF/MMA–SSA7:3 and copolymer MMA–SSA7:3.

3.3. Morphology of the DF/MMA–SSA membranes

Pursuant to the illustration shown in Fig. 4, the XRD investigation of the three selected membranes provides useful information about (1) the phase structures of this triple component blend, and (2) the association between DF and MMA, which was weakened with the increase in SSA content in the copolymer (Fig. 6). The XRD of DF/MASA9:1 shows one peak at $2\theta = 20.5°$, which represents the crystalline PVDF phase, and a shoulder peak at $2\theta = 14.5°$. Also, the shoulder peak moves to $2\theta = 17.5°$ in the XRD of DF/MASA8:2. This shift of 2-theta suggests that the shoulder peak come from the perturbed crystalline DF phase due to the engagement

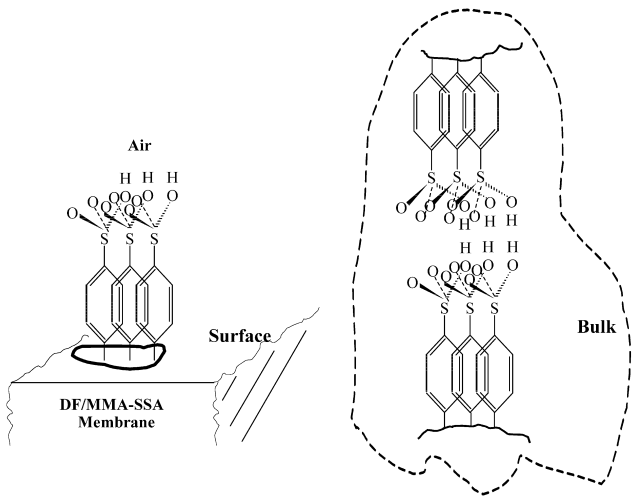

Fig. 3. An illustration of the ordered assembly of SSA units in the DF matrix.

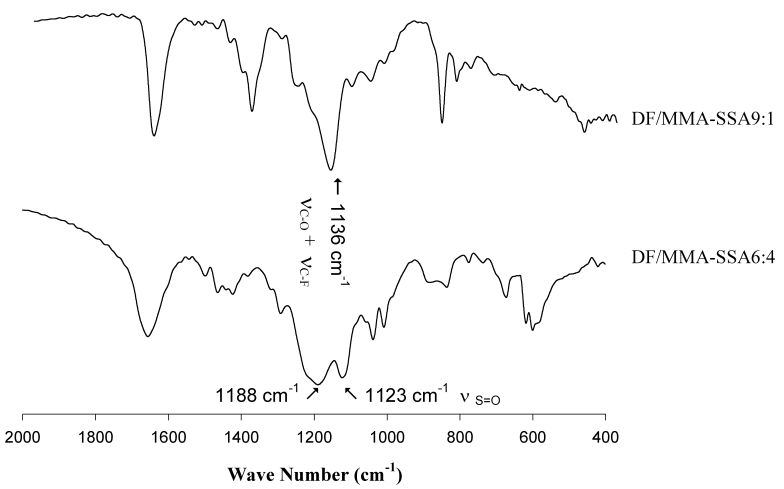

Fig. 4. FT-IR spectra of two different membranes.

with MMA segments. In addition, the shoulder peak became weaker with the increase in the SSA content and eventually disappeared in the XRD pattern of DF/MASA6:4, the sample containing the highest SSA content of the three. This is an indicative of the lowest extent of MMA-DF interaction. It is supposedly due to the contraction of a large number of SSA segments in the membrane with a relatively lower content of MMA.

As to the dispersion of SSA segments in the matrix of membrane, we examined the cross-section of the membranes (obtained by rupturing it in liquid N_2) by SEM both at low and high magnifications. When inspected at the low magnification (Fig. 7(a) and (b)), EDX scan across the fractural section of DF/MMA–SSA6:4 membrane showed that its atomic concentration profile of sulfur is as uniform as what happens in the Nafion®-117 membrane (Table 2). The SEM cross-section features of these two types of membranes are very different; Nafion displays a clearly ruptured morphology but DF/MMA–SSA6:4 does not. This also reflects the unique matrix structure of the partially miscible blend. On the other hand, under the scrutiny at the high magnification, a SEM image consisting of bright spots and the normal texture morphology was observed (Fig. 8). The EDX probing showed that these bright domains represent locations of the assemblies of SSA segments as shown in Fig. 3. A much higher sulfur concentration was detected at these domains than on the surrounding matrix, and a nil fluorine concentration was found whereon. According to the sizes of these bright domains, the SSA assemblies in the dry matrix have a dimension of about 100 nm. It may need to note that the morphologies of Fig. 8 represent the cross sections of the membranes instead of the surface of casting membranes. Hence, they are relevant to the analysis in the following part of the proton conduction across the electrolyte membrane.

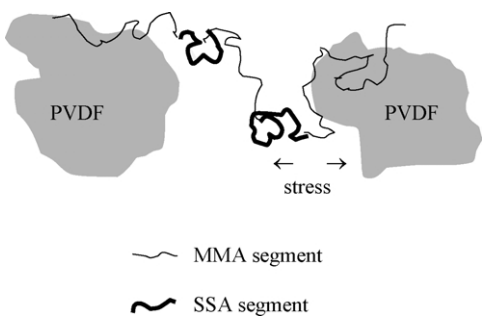

Fig. 5. An illustration of the dual affinity of MMA–SSA in the DF matrix.

3.4. Proton conductivity

Proton conductivity of the membranes made of the copolymers or the blends has been evaluated employing the impedance spectroscopy. The measurement was conducted in a rather wide span of frequency from 1 to 10 MHz. All the samples were saturated with de-ionized water prior to the measurement; Fig. 9 shows the saturated water contents in the four different DF/MMA–SSAi : j membranes at about

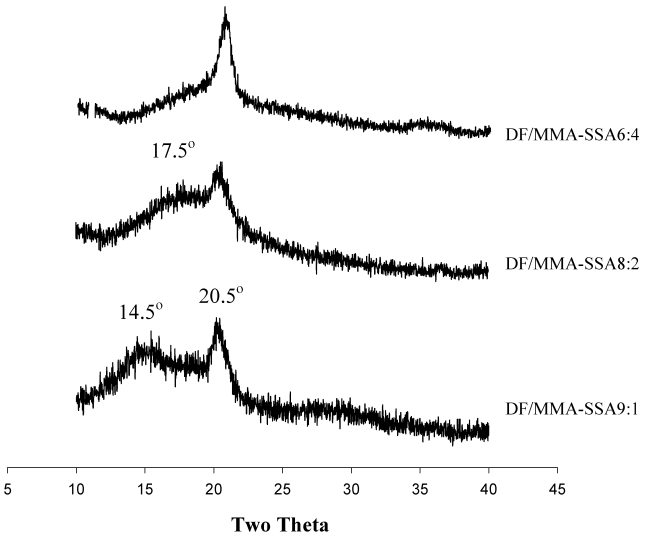

Fig. 6. XRD diagrams of DF/MMA–SSA9:1; DF/MMA–SSA8:2 and DF/MMA–SSA6:4.

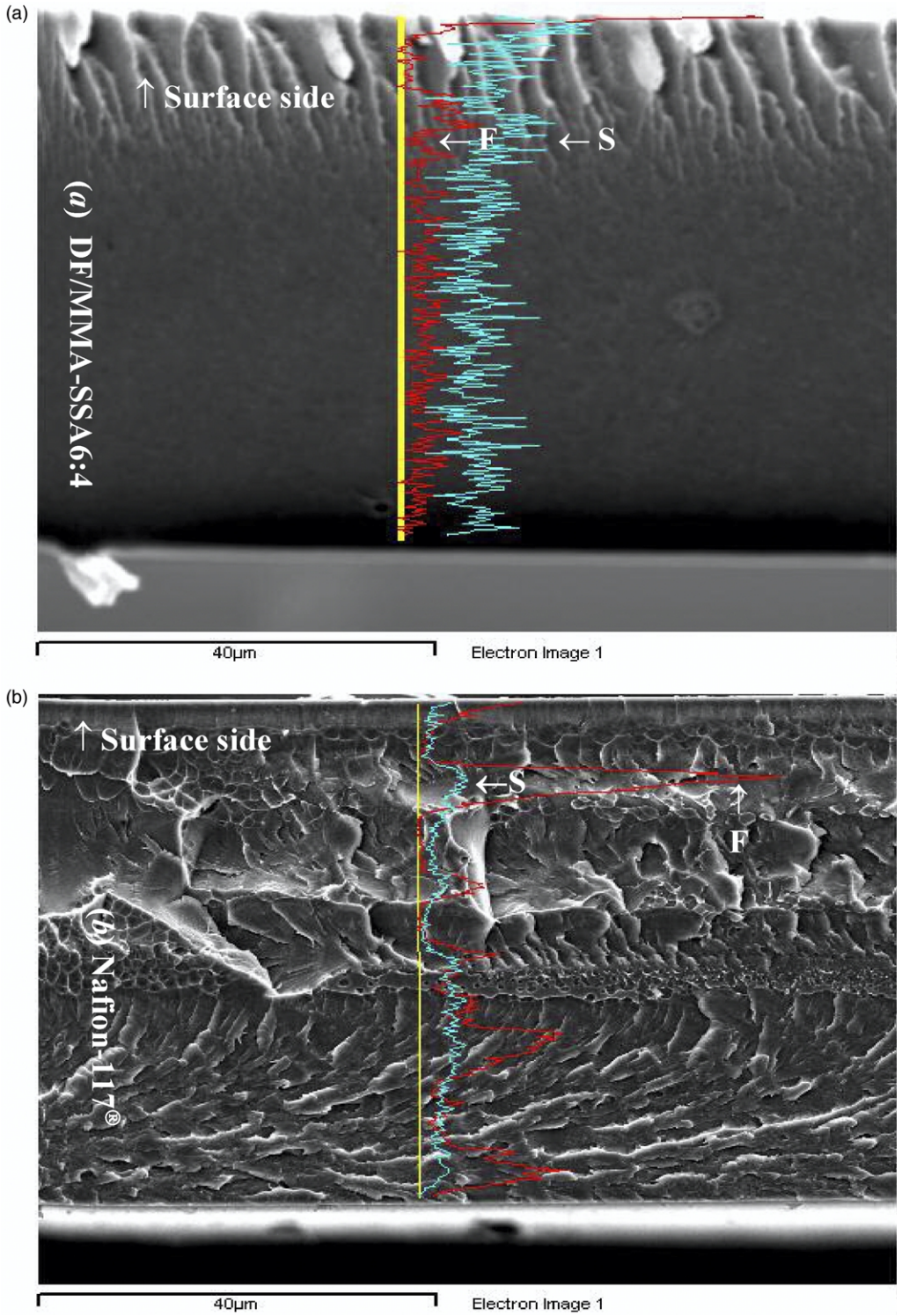

Fig. 7. Cross-sectional EDS elemental profiles: (a) DF/MMA–SSA6:4 and (b) Nafion®-117.

25 °C. As expected, the extent of hydration rises with increasing SSA content in the copolymer and hence in the corresponding membrane.

The impedance measurement shows that the conductivity (based on Z'_b value, it will be defined later) of the copolymers change from 2×10^{-3} to 4.1×10^{-2} S cm^{-1} in line with the change of SSA content from about 11 to 36 wt% (Fig. 10). Despite having very high proton conductivity, the copolymer is an unqualified PEM because of its poor dimensional stability. For instance, it is easy to be swollen and eventually dissolved in water when SSA content is around 36 wt%. Blending the proton-conductive

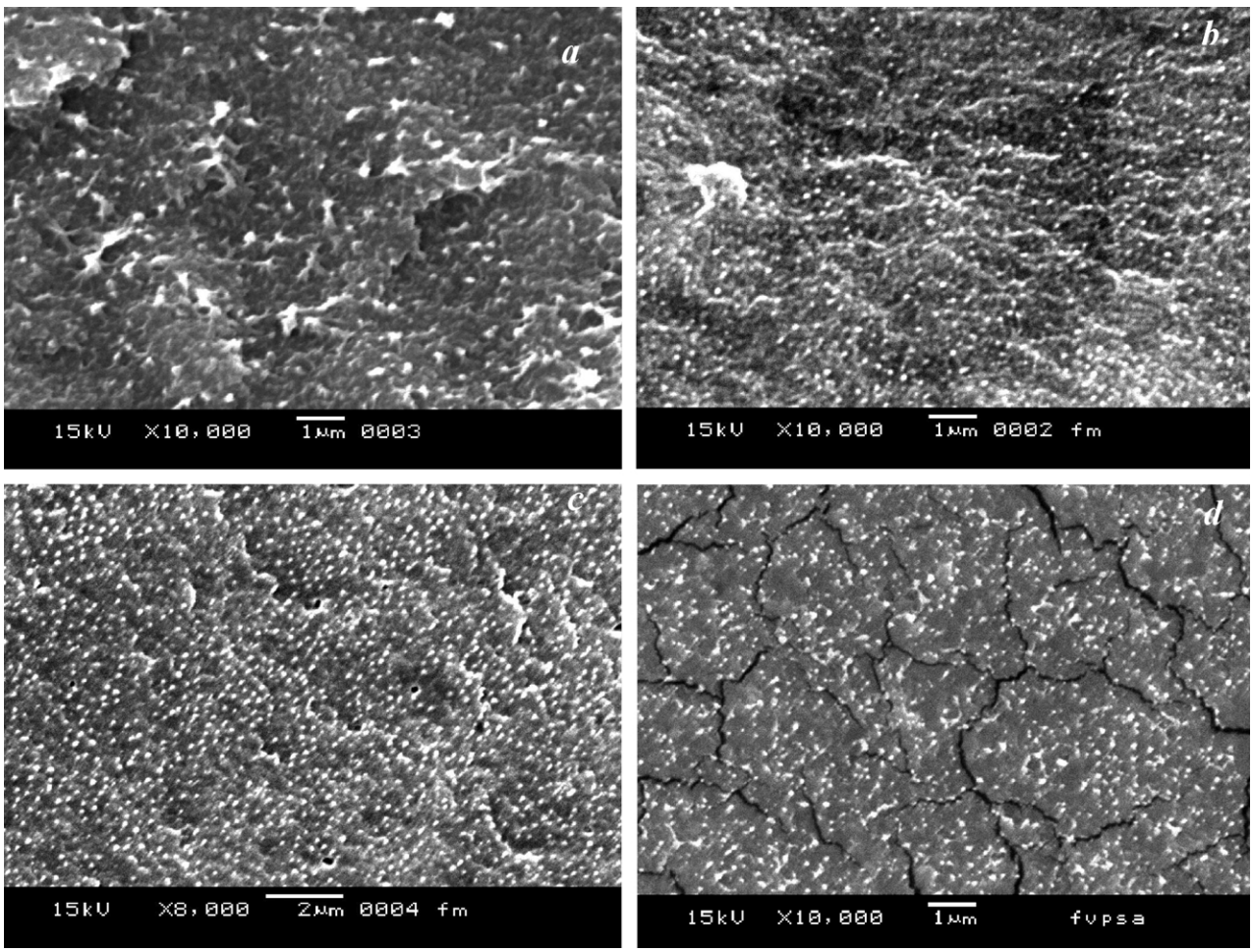

Fig. 8. SEM images of the cross section of the membranes: (a) DF/MMA–SSA9:1; (b) DF/MMA–SSA8:2; (c) DF/MMA–SSA7:3; (d) DF/MMA–SSA6:4.

component with semi-crystalline DF is an effective approach to circumvent this problem, as it is well known to have good mechanical properties. Being a hydrophobic polymer, DF constitutes a barrier to the proton motion. As a result, a large boost of the proton conductivity happened accompanying with the increase in SSA content in the membrane from DF/MMA–SSA9:1 to DF/MMA–SSA8:2 (see Table 2 for the SSA contents). On inspection of their matrix morphology, one could observe a morphology transition in which submicro-domains of the SSA assemblies began to appear since DF/MMA–SSA8:2 (Fig. 8(b)). This could be taken as the root-cause for the above 'percolation threshold' phenomenon. Although the conductivity is proportional to the content of SSA, there is an optimal SSA content at which the mechanical property of membrane could be balanced. As shown in Fig. 4, the two monomer units in MMA–PSS copolymer own the opposite affinities with the DF polymer; the repulsion causes material stress in the membrane. Hence, too high a SSA content, such as in DF/MMA–SSA6:4, will aggravate the situation, resulting in micro-cracks throughout the membrane (Fig. 8(d)). In this connection, membrane DF/MMA–SSA8:2 is a more suitable membrane than DF/MMA–SSA7:3 because both have similar proton conductivity ($\sim 10^{-3}$ S cm^{-1}) but the former has a higher DF content and, therefore, better mechanical strength despite the fact that both are free standing. It is noteworthy that the above two membranes show a proton conductivity range that is quite close to what Nafion$^{@}$-117 offers (10^{-2} S cm^{-1}). This result implies that the discrete SSA domains may overreach upon hydration to form a certain sort of connection.

The experimental impedance spectrum of a solid electrolyte often consists of a semi-circle arc, a linear segment and a transition zone between the two. The spectrum is usually interpreted by an equivalent electrical circuit comprising a resistance and an impedance of electrode process in series. Hence, the in-phase (Z') and out-of-phase (Z'') components of the impedance can be figured out. The arc intercepts the horizontal (Z') axis at two points: they are Z'_b at high frequency side and Z'_i at the low frequency side, respectively, with $Z'_b < Z'_i$.. Value Z'_b represents the pure resistance of the electrolyte according to the above equivalent RC circuit; the diameter of the arc ($Z'_i - Z'_b$) reflects the resistance to charge transfer at the electrode. On the other hand, the value obtained from the extrapolation of the linear line to the real axis represents

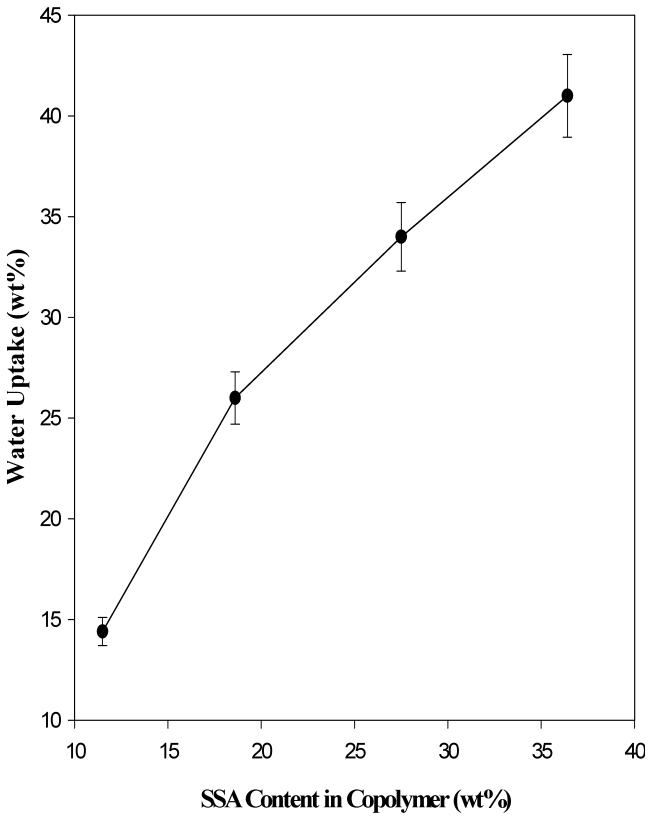

Fig. 9. The effect of SSA content in the membranes on their water uptake, all the results stands for the saturating capacities at 25 °C.

the diffusion of charge carriers through the electrolyte and arrival to the electrode, known as the Warburg impedance.

It has been known that the matrix of DF/MMA–SSA membranes is a heterogeneous medium. The interface between the SSA domains and the surrounding matrix can be envisaged as a capacitor. Hence, the above equivalent circuit for the electrolyte in the measurement cell should be slightly amended to have a pure resistance (Re) plus one capacitor (Ci) in series (Fig. 11). The impedance of the electrode process can be broken up to three elements; they are the capacitor simulating the membrane/electrode interface (Cd), the resistance to charge transfer (Rct) and the resistance to mass transport of protons (Z_w) at this interface.

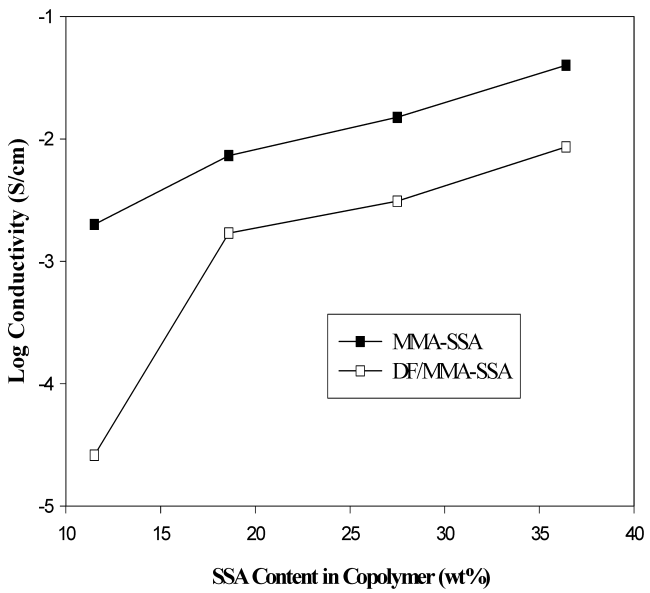

Fig. 10. The effect of SSA content on proton conductivity (■) MMA–SSA; (□) DF/MMA–SSA.

Following the preceding discussion, Z_i' is equivalent to Re, reflecting the extent at which protons could migrate across the DF phase that separates the SSA domains, $Z_i' - Z_b'$ is equivalent to Rct. The proton conductivity of the membrane relies on the dispersion density of SSA domains in the matrix. Fig. 12 shows the effect of SSA content on the impedance spectra of the three membranes. In this measurement, the three membranes absorbed the saturated contents of water as indicated in Fig. 9. The impedance spectrum of membrane DF/MMA–SSA9:1 shows the typical Sluyters plot, in which the semi-circle should embrace the capacitive resistances from the two interfaces (Ci and Cd). From the spectrum, Z_i' ($\sim 20\,\Omega$) and Z_b' ($\sim 200\,\Omega$) could be clearly found. With increasing SSA content to 10.3% (Table 2), the impedance of membrane DF/MMA–SSA8:2 shows no sign of the semi-circle but a straight line having a slope very close to $\tan \pi/4$ and intercepting with Z' axis at about $20\,\Omega$. The straight line, known as the Warburg impedance, corresponds to the electrode reaction controlled only by the mass transfer of protons since the resistance to charge transfer at electrode becomes very small ($Z_i' - Z_b' = 0$). Compared with DF/MMA–SSA9:1, an enhancement of the mass transfer of protons also happened in membrane DF/MMA–SSA8:2, that is, the intercept of the straight line at Z' axis is much smaller ($230\,\Omega$ vs. $20\,\Omega$). This trend continues in the membrane DF/MMA–SSA6:4 and can be explained by the ease with which mutual interconnecting SSA channels could be formed. When the SSA domains were swollen by water, the interval between SSA domains could be bridged through entanglements of hydrated SSA segments. The higher the SSA matrix density the easier the inter-links would be created. This explanation can also find support from the fact that the semi-circle shrank to a dot when moving from membrane 9:1 to membrane 8:2; it is an indicative of the removal of the isolation state of SSA phase in the DF/MMA–SSA matrix.

The response of proton conduction to the water uptake in the membranes has also been studied using membrane DF/MMA–SSA8:2 as the example. Fig. 13 shows that two different impedance diagrams corresponding to two respect-

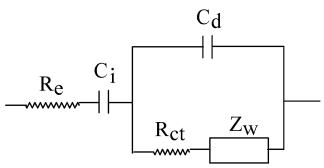

Fig. 11. The equivalent electric circuit of the electrochemical measurement device of DF/MMA–SSA membranes.

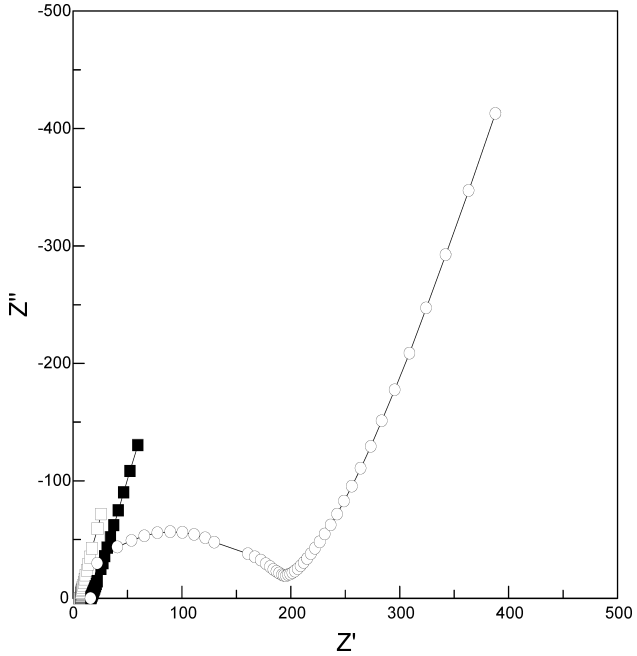

Fig. 12. The impedance spectra of (○) DF/MMASSA9:1; (■) DF/MMASSA8:2; (□) DF/MMASSA6:4.

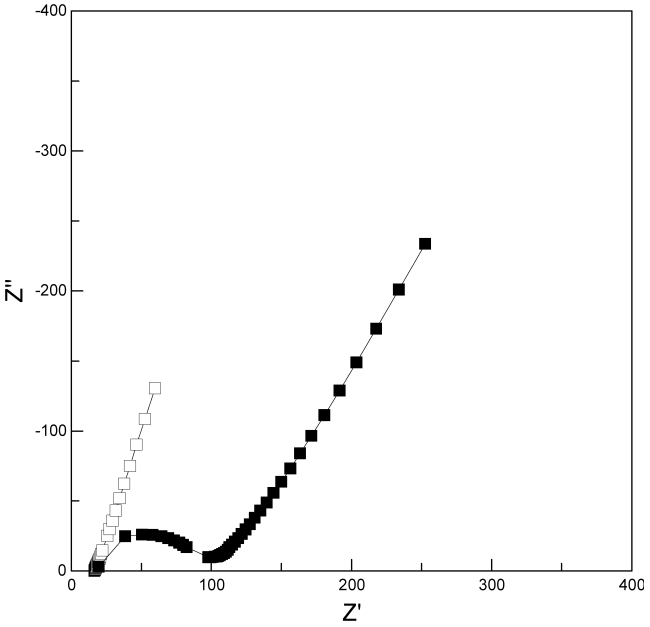

Fig. 13. The impedance spectra of DF/MMASSA8:2 containing (□) 26 wt%; (■) 11 wt% water.

ive water uptake levels. At a lower water-content (11 wt.%), the Sluyters plot is obtained, however, when water content moves up to 26%, the Warburg impedance appears instead. This observation further proves the above explanation in the sense that the SSA segment motion required an adequate water uptake. At the lower water content, the interfaces existing in the membrane matrix and between the membrane and the electrode could not be effectively 'short circuited' by the linking of movable SSA segments, so the semi-circle was still displayed.

Finally, regarding the effect of the SSA content on the reduction of the resistance to proton diffusion, the two Warburg impedances (in the Fig. 12) show quite similar resistances to the proton diffusion (the intercepts of the straight lines at Z' axis) despite one fold of the difference in their SSA contents (Table 2). This implies that to further improve proton conductivity, something else should be done instead of bringing up the SSA content. It looks like that strong hydrophobicity of the benzene ring of SSA is the key factor causing the problem.

4. Conclusions

The copolymer poly(methylmethacrylate-co-styrenesulfonic acid), MMA–SSA, synthesized via solution polymerization, was made up of random segments of the two monomer units. When the copolymer was blended with poly(vinylidene floride), DF, SSA segments could be distributed very uniformly over the DF matrix, forming nano-scale domains. The resultant membrane, composed of the hydrophobic PVDF phase, the hydrophilic SSA phase, and the MMA phase as the intercession, is free standing when saturated with water. The high dispersion of SSA segments in the membrane is the crucial feature that ensures a fast proton transport mechanism. In this type of proton electrolyte membrane, there is an optimum content of SSA, over which the resulting membrane will become fragile and no substantial increase in proton conductivity could be gained as well.

References

[1] Hsu WY, Gierke TD. J Membr Sci 1983;13:307–26.
[2] Gupta B, Scherer GG. Angew Makromol Chem 1993;210:151–64.
[3] Holmberg S, Lehtinen T, Näsman J, Ostrovskii D, Paronan M, Serimaa R, Sungholm F, Sundholm G, Torell L, Torkkeli M. J Mater Chem 1996;6(8):1309–17.
[4] Mattsson B, Ericson H, Torell LM, Sundholm F. J Polym Sci, Part A: Polym Chem 1999;37(16):3317–27.
[5] Pimbert S, Avignon-Poquillon L, Levesque G. Polymer 2002;43(11): 3295–302.
[6] Sasaki H, Bala PK, Yoshida H, Ito E. Polymer 1995;36(25):4805–10.
[7] Moussaif N, Jerome R. Polymer 1999;40(14):3919–32.
[8] Jouannet D, Pham TN, Pimbert S, Levesque G. Polymer 1997;38(20): 5137–47.
[9] Odian G. Principles of polymerization, 3rd ed. New York: Wiley; 1991. Chapter 6.
[10] Rogers SC, Mackrodt WC, Davis TP. Polymer 1994;35(6):1258–67.
[11] Weiss RA, Lundberg RD, Turner SR. J Polym Sci, Polym Chem Ed 1985;23:549.
[12] Hietala S, Koel M, Skou E, Elomaa M, Sundholm F. J Mater Chem 1998;8:1127–32.
[13] Glipa X, Haddad ME, Jones DJ, Rozière J. Solid State Ionics 1997;97: 323–31.
[14] Pouchert CJ, Aldrich library of FT-IR spectra, vol. 2. Wisconsin, WI: Aldrich Chemical Co; 1985.